Hierarchical velocity structure in the core of Abell 2597

Martin Still[1] and Richard Mushotzky
NASA/Goddard Space Flight Center, Code 662, Greenbelt, MD 20771

ABSTRACT

We present *XMM-Newton* RGS and EPIC data of the putative cooling flow cluster Abell 2597. Velocities of the low-ionization emission lines in the spectrum are blue-shifted with respect to the high-ionization lines by $1\,320^{+660}_{-210}$ km s^{-1}, which is consistent with the difference in the two peaks of the galaxy velocity distribution and may be the signature of bulk turbulence, infall, rotation or damped oscillation in the cluster. A hierarchical velocity structure such as this could be the direct result of galaxy mergers in the cluster core, or the injection of power into the cluster gas from a central engine. The uniform X-ray morphology of the cluster, the absence of fine scale temperature structure and the random distribution of the the galaxy positions, independent of velocity, suggests that our line of sight is close to the direction of motion. These results have strong implications for cooling flow models of the cluster Abell 2597. They give impetus to those models which account for the observed temperature structure of some clusters using mergers instead of cooling flows.

Subject headings: galaxies: clusters: individual: A2597 – galaxies: distances and redshifts – X-rays: galaxies

1. Introduction

It has long been theorized (Burns et al. 2002) that the formation of clusters by hierarchical mergers would produce velocity substructure in the X-ray emitting gas in clusters of galaxies. However the observational consequences of such substructure is not clear and several detailed simulations differ in their predicted amplitude and detailed structure (c.f. Roettiger & Mushotzky, 1998; Norman & Bryan 1999; Nagai & Kravtsov 2003; Onuora, Kay and Thomas 2003). The predicted structures range from generalized turbulence, the existence of large velocity structures, the signature of the infall of an individual group, rotation and infall along the filaments which meet at the cluster. Despite this uncertainty, the general existence of velocity structure is a strong prediction of hierarchical merging. The other possible source of velocity structure is the action of an AGN in the center of the galaxy which can put mechanical energy into the gas via the production of jets, radio "bubbles" or other unspecified means, producing bulk motion and turbulence (e.g., Churazov et al. 2000, Reynolds, Heinz and Begelman 2002, Fabian et al. 2003).

Thus, while long predicted, the only evidence to date for the existence of such motion is the suppression of resonance scattering in several clusters and galaxies (Xu et al. 2002; Gastaldello & Molendi 2004; Churazov et al. 2004) and the shapes of head-tail cluster radio sources (Burns et al. 2002). The relative level of resonance scattering suppression implies fairly strong turbulence or velocity shear with a Mach speed $> 1/3$ of the sound speed in the X-ray emitting gas associated with the radio sources in M87 and the Perseus cluster. However in the only data so far published of a radio quiet giant elliptical galaxy, NGC 4636, there is a strong upper limit on turbulence or velocity shear (Xu et al. 2002). There is, at present, no strong evidence for velocity structure in the X-ray emitting gas in other clusters, groups or galaxies (but see Bregman and Dupke 2002 for possible large scale velocity structure in the Perseus and Centaurus clusters).

[1]Universities Space Research Association

In this paper we report the detection with the *XMM-Newton* RGS gratings of velocity substructure in the core of of the rich cluster Abell 2597, one of the "massive cooling flow clusters" (Crawford et al. 1989). This velocity structure is consistent with the observed redshift distribution of the galaxies. Rather than a cooling flow, we believe that this data supports the merger model (Motl et al. 2004) for the origin of the cool gas in this cluster.

2. Observations

XMM-Newton (Jansen et al. 2001) observed Abell 2597 between 03:29 UT and 09:20 UT on Nov 30, 2000[2]. EPIC, RGS and OM cameras were in operation; see Strüder et al. (2001), Turner et al. (2001), den Herder et al. (2001) and Mason et al. (2001) for instrument details. Raw Observation Data Files files were reprocessed using the pipeline software distributed within SAS v5.4 and spacecraft calibrations which were up-to-date as of Dec 11, 2003. Since there was no significant proton-induced background flare activity during the exposures, additional time-screening was not required.

The EPIC MOS and EPIC pn cameras were operated in full-frame mode behind medium filters. Event files were screened for known and new bad pixels, and events of complexity greater than doubles were rejected. Events with corrected pulse heights below 300 eV were screened out to avoid calibration uncertainties.

RGS first order spectra were extracted from a source position of RA=351.33229 and Dec=-12.12389 using channel binning of 0.045Å. The cross-dispersion extraction region was defined to include 98 percent of the flux within the RGS cross-dispersion Point Spread Function (PSF). The shape of the cross-dispersion PSF is variable over the dispersion axis, with the extraction region ranging in width between 2.2–3.8 arcmin. With a 5 arcmin field of view in the cross-dispersion direction, this allowed sky regions to be extracted, albeit with reduced signal-to-noise compared to point source data and with some small contamination from the faint, outer regions of the cluster. Due to the small number of events, second order spectra are not analyzed.

[2]Observation ID: 0108460201

3. EPIC results

We performed imaging spectral analysis of Abell 2597 in the central 6 arcmin, where the surface brightness exceeds the internal background. Extracting events from concentric annuli about the cluster center and fitting collisional plasma models (Brickhouse et al. 2000), we measure an average overall temperature of 3.5 keV consistent with the ASCA average temperature and evidence for a temperature drop in the central 50 arcsec, consistent with the Chandra results of McNamara et al. (2001). While our temperatures are statistically more precise than those of McNamara et al. , the poorer angular resolution does not allow full resolution of the central temperature profile. The X-ray color map shows little evidence for spatial temperature structure other than the overall reduction in temperature in the central 45 arcsec. The source was found to be isothermal at radii > 1 arcmin from the center with no abundance gradients. In Fig. 1 we plot the temperature map, with intensity contours overlayed, and the best-fit temperatures and Fe abundances versus angular distance from the cluster core.

4. RGS results

First order RGS spectra of Abell 2597 are plotted in Fig. 2, revealing emission lines of O VIII Lyα, L-shell Fe transitions and, marginally, Si XIV Lyα.

4.1. Emission line velocities

Because the target source is extended, there is a range of incident angles on the gratings and emission lines are consequently broadened. In order to fit the line profiles adequately we must simulate the instrumental broadening. The simplest method is to convolve a model spectrum with the integrated spatial profile of the source collapsed in the cross-dispersion direction of the RGS cameras, producing a convolution function for the model. This is achieved with the model *rgsxsrc*, added to the XSPEC package for version 11.2. In this case we have used a 0.35-2.5 keV image, extracted from the EPIC MOS1 events list to generate the function. Although fast computationally, the disadvantage

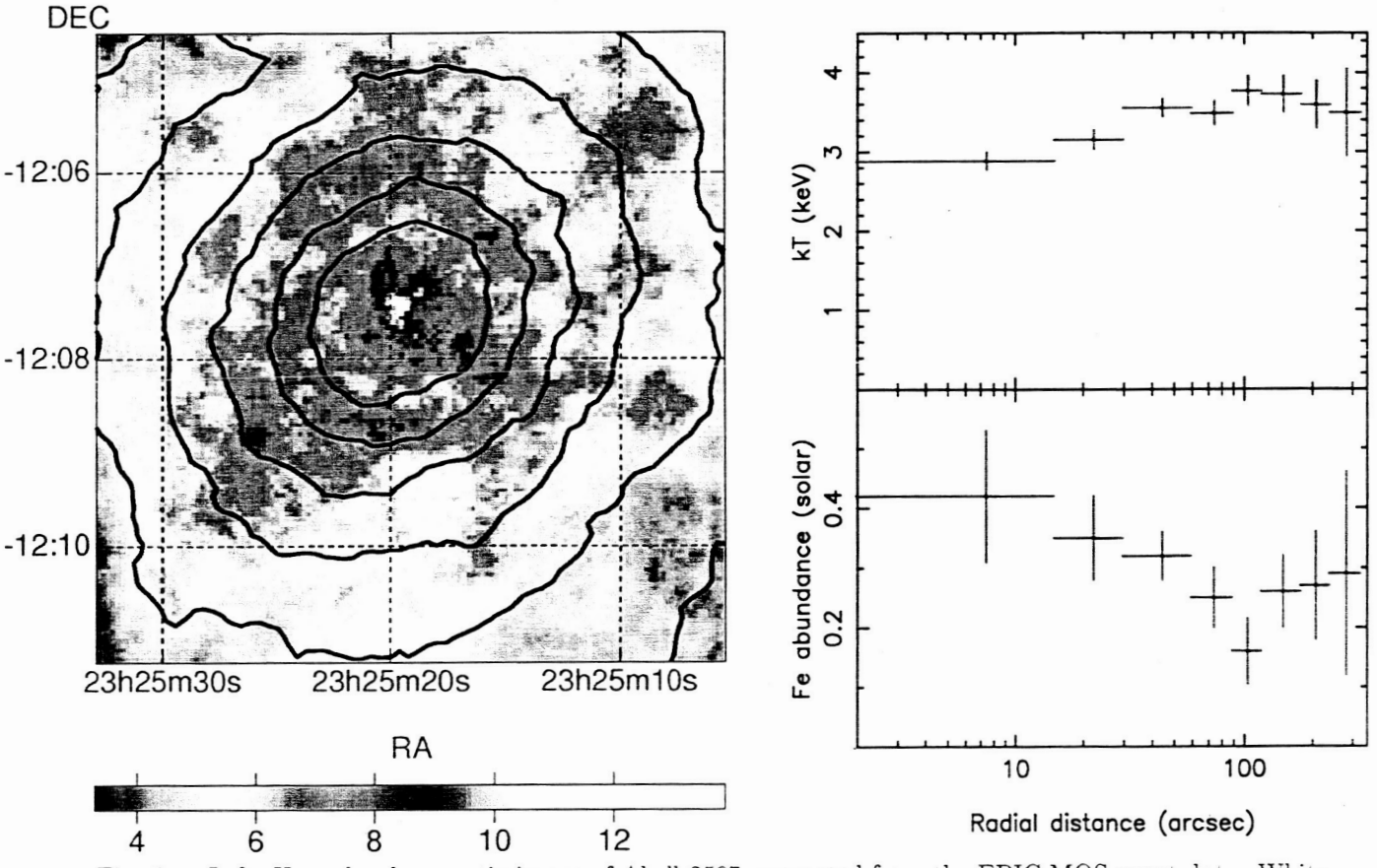

Fig. 1.— Left: X-ray hardness ratio image of Abell 2597, extracted from the EPIC MOS event data. White to red indicates increasing temperature. The bands employed in the calculation were 0.3–2 keV and 3–8 keV with images smoothed by a factor ??? using Gaussian convolution. Counts of 6–8 per pixel correspond to blackbody temperatures of 3.6–4.6 keV, 8–10 counts to 2.9–3.6 keV and 10–12 counts to 2.5–2.9 keV. X-ray intensity contours from an unsmoothed 0.3–2 keV image combined from MOS1 and MOS2 are superposed over the image. Right: Collisional plasma fits to EPIC spectra extracted from concentric annuli around the cluster core. We plot plasma temperature and Fe abundance as functions of angular distance from the core.

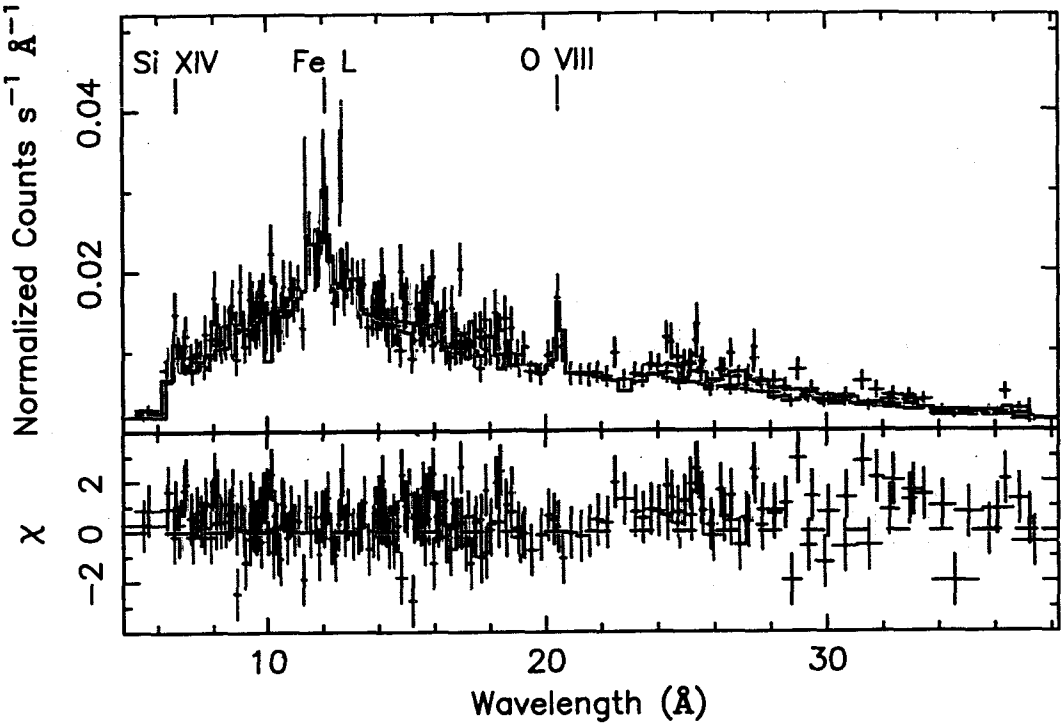

Fig. 2.— *XMM-Newton* RGS1 (blue) and RGS2 (red) spectra of Abell 2597. The black lines correspond to the best-fit two-temperature collisional plasma model, described in Sec. 4. Lines from O VIII, Fe XXIII (or Fe XXII), Fe XXIV, and possibly Si XIV are detected. The bottom panel plots the fit residuals.

of this method is that the emitted spectrum is assumed to be isothermal across the source.

To measure the redshift of the O VIII Lyα line we use a Gaussian model, with a powerlaw to represent the continuum across the wavelength range 19–22Å. The best fit model, convolved with the spatial profile above, is plotted in Fig. 3. We take the rest-energy of the line as 653.6 eV (Johnson & Soff 1985) and assume that the local intrinsic width of the line is negligible. The redshift of this feature is consequently $z = 0.081^{+0.002}_{-0.004}$ ($\chi^2 = 51$ for 52 d.o.f.), where the errors are 90 percent confidence limits. This is less than the commonly cited mean optical redshift of the cluster $z = 0.0852$ (Struble and Rood 1999) with greater than 99 percent confidence.

An identical model, ray-traced through a simulation of the *XMM-Newton* telescope using the Monte Carlo code discussed in Peterson et al. (2001), yields a consistent fit of $z = 0.078 \pm 0.001$. While the result is not particularly sensitive to the spatial distribution of the source, based on the broad band EPIC MOS image, we assumed the O VIII line is distributed as a β-function, where the spatial profile has an index of 0.62 and core radius of 27 arcmin.

A convolved Gaussian plus powerlaw model fit to the suspected Lyα Si XIV line over the $\lambda\lambda$5–8Å range provides $z = 0.078^{+0.006}_{-0.009}$ ($\chi^2 = 52$ for 52 d.o.f.), taking the rest wavelength as 2.005 keV (Johnson & Soff 1985). This is consistent with the O VIII redshift and, again, inconsistent with the Struble and Rood redshift with 90 percent confidence.

To fit the Fe L shell transitions we adopt a neutrally-absorbed thermal plasma model (*vapec*; Brickhouse et al. 2000) over $\lambda\lambda$8–15Å, convolved with the EPIC MOS1 spatial profile. Photo-electric cross-sections were provided by Balucinska-Church & McCammon (1992). Best fit parameters are $z = 0.086^{+0.004}_{-0.005}$, $n_{\rm H} = 4^{+6}_{-4} \times 10^{20}$ cm^{-2} and $kT = 3.1^{+1.0}_{-0.8}$ keV, with an Fe abundance of $0.44^{+0.32}_{-0.19}$ solar ($\chi^2 = 189$ for 179 d.o.f.). The velocity of the Fe emission is consistent with both the Struble and Rood optical redshift of the cluster and the O VIII line within the 90 percent confidence limits. However there is one strong line at λ12.7Å that is not fit well by the model. This is partly because it is both blue-shifted relative to the best-fit velocity and narrower than the

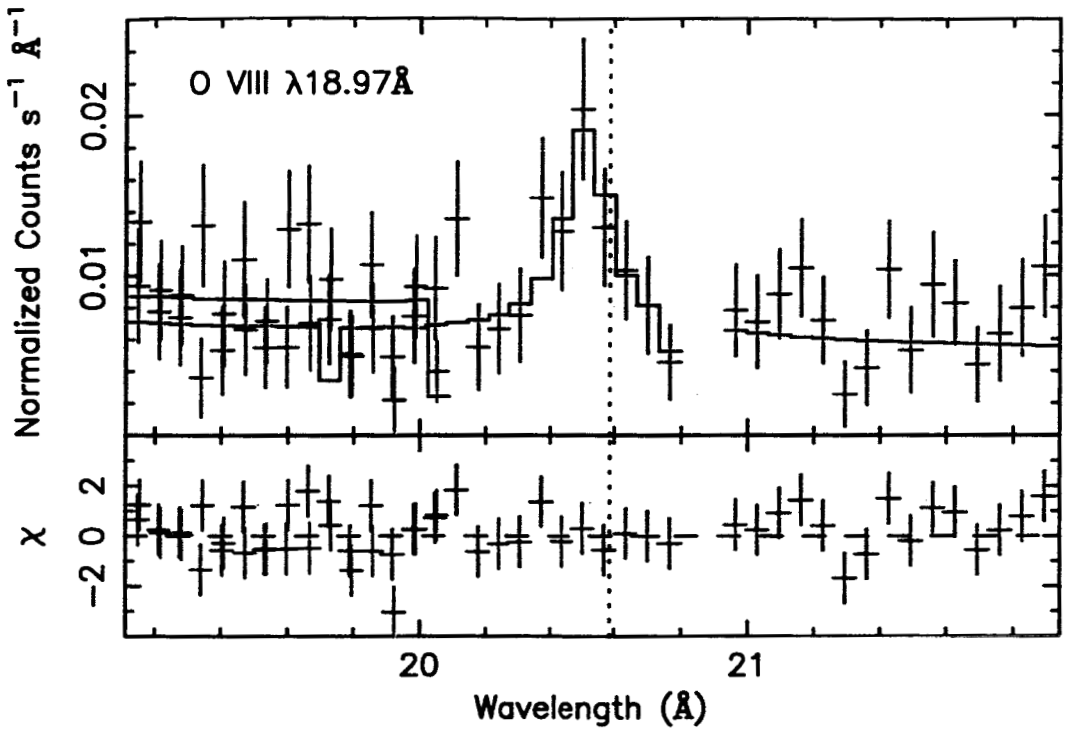

Fig. 3.— RGS1 (blue) and RGS2 (red) spectra of the O VIII line from Abell 2597. The black lines correspond to a powerlaw + Gaussian fit, convolved with the 0.35–2.5 keV EPIC MOS1 spatial profile. The redshift of the line corresponds to $z = 0.081$, whereas the mean optical redshift is represented by the vertical dotted line. The lower panel plots fit residuals.

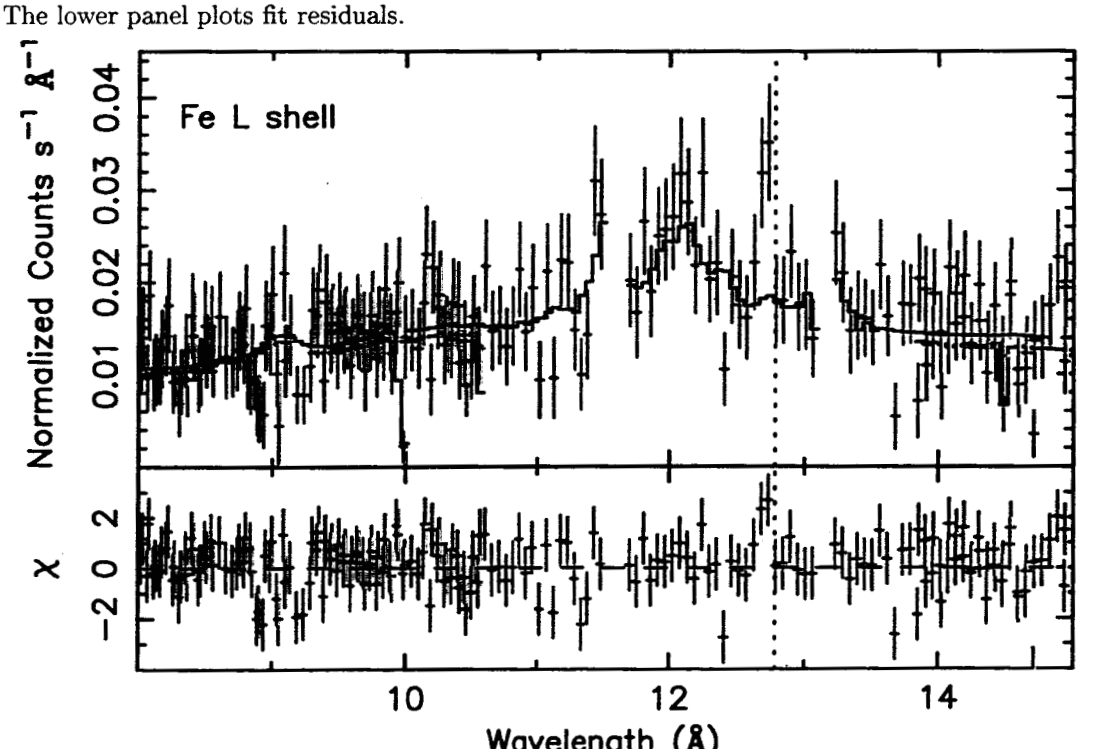

Fig. 4.— RGS1 (blue) and RGS2 (red) spectra of the Fe L complex from Abell 2597. The black lines correspond to an absorbed thermal plasma model (*vapec*) fit, convolved with the 0.35–2.5 keV EPIC MOS1 spatial profile. The lower panel plots fit residuals, including a narrow line of either Fe XXII or Fe XXIII at λ11.7Å. The wavelength of these lines moved to the mean optical redshift of the cluster is represented by a vertical dotted line.

EPIC MOS1 convolution function. An additional line with negligible intrinsic width was added to the model and fit to this feature. It is likely this line is either Fe XXII λ11.770Å at $z = 0.080^{+0.004}_{-0.004}$ or Fe XXIII λ11.736Å at $z = 0.082^{+0.004}_{-0.004}$ (Brown et al. 2002).

The RGS2 chip gap between $\lambda\lambda$13.1–13.2Å may overlap another strong line. The current model is fitting solar abundance Ne X Lyα to the red wing of the feature, but this line equally may be Fe XXI λ12.284Å, which would reduce the temperature of the model considerably. By removing Ne from the model completely, best fit thermal plasma parameters are $z = 0.085^{+0.003}_{-0.006}$, $n_{\rm H} = 9^{+12}_{-4}\times10^{20}$ cm^{-2} and $kT = 2.0^{+0.6}_{-0.6}$ keV, with an Fe abundance of $0.22^{+0.14}_{-0.10}$ solar ($\chi^2 = 187$ for 179 d.o.f.).

The temperature is still too high to produce significant amounts of Fe XXI (Arnaud & Rothenflug 1985), but this is not especially surprising. In reality, the source has a range of plasma temperatures (Sec. 4.2), while the fit above converges on a mid-range value. The quoted temperature is also artificially high because the narrow Fe XXII/Fe XXIII line is not being fit correctly by the instrumentally-broadened model. What we can say with some certainty is that in collisional conditions, the absence of ionization states with energies equal or less than Fe XX indicates plasma temperatures > 1 keV, while if Fe XXII is the cutoff state, the plasma temperature must be > 1.5 keV (Arnaud & Rothenflug 1985).

In summary, the hot Fe XXIV lines have velocities consistent with the Struble & Rood (1999) optical redshift of the cluster. The unblended O VIII and Si XIV Lyα lines are blueshifted relative to this velocity with > 90 percent confidence. The velocity of the cooler Fe transition, either Fe XXII or Fe XXIII, is statistically more consistent with the O VIII and Si XIV and is narrower than the Fe XXIV lines, suggesting an origin within a localized region of the cluster.

4.2. A two-zone model

Fe transitions of different widths suggest that these lines are spatially distributed differently in the source. The Fe line widths are as expected phenomenologically for a cooling flow – the broad lines arise in a large, hot outer volume while the narrow lines originate in the cooler, inner flow. This model explain explains elegantly why the O and Si lines are broad, yet display the peculiar velocity of the cool core. Whereas the Fe XXII and Fe XXIII ionization states emit over relatively narrow distributions in temperature, H-like O and Si have distributions considerably broader, with ranges encompassing Fe XXI–XXIV. Consequently, the O and Si lines should arise in both the inner and outer regions of the source.

A first order approximation to this picture is a two-zone model. The outer zone is an extended thermal plasma which we model using the EPIC MOS1 convolution function to broaden the spectra. The inner zone is a thermal plasma, modeled as a point source. Both zones are absorbed by the same galactic neutral hydrogen column in the direction of the source, $n_{\rm H} = 2.49\times10^{20}$ cm^{-2} (Dickey & Lockman 1990).

Plasma parameters for the outer zone were fixed at values determined from the EPIC data (Sec. 3). We take $kT_{\rm o} = 3.5$ keV and element abundances [Fe/H] = −0.52 and [O/H] = −0.32. The suffix "o" corresponds to the outer region of the model. Since the source was found to be isothermal at radii > 1 arcmin from the center with no abundance gradients, our choice of an isothermal convolution template is vindicated. Free floating parameters for this component are the normalization and the Si abundance which, being poorly constrained by the EPIC data, is tied to the Si abundance of the point source component in order to reduce redundancies. The temperature, $kT_{\rm i}$, Fe, O and Si abundances, and normalization of the inner zone component are also free floating parameters. The velocities of the two zones are initially coupled, yielding a best-fit redshift for the cluster of $z = 0.083^{+0.002}_{-0.004}$ ($\chi^2 = 185$ for 179 d.o.f.). This value is not consistent with the Struble and Rood (1999) optical redshift within the 90 percent confidence limits. Furthermore, the formal chi^2 is driven mostly by optically thin continuum which is insensitive to the redshift. This current fit represents the velocities of the O VIII and Fe XXIII lines poorly.

The fit to these lines improves if we decouple the redshift of the two zones. First, by fixing the redshift of the outer zone to the Struble and Rood value, $z_{\rm o} = 0.0852$. The best-fit inner zone redshift in this case is $z_{\rm i} = 0.0808^{+0.0007}_{-0.0022}$ ($\chi^2 = 184$ for 179 d.o.f.). Best fit parameters for this

model are provided in Table 1, and the best fit model spectrum is plotted over the data in Fig 2. $z_i = 0.0808^{+0.0007}_{-0.0022}$ is less than the mean optical redshift with 8σ confidence. Conversely if we fix z_i at 0.0808, $z_o = 0.090^{+0.006}_{-0.008}$ ($\chi^2 = 183$ for 179 d.o.f.)

For comparison, a two zone model applied to the central 1 arcmin of the EPIC data gives a best fit temperature of $kT_i = 1.7^{+0.1}_{-0.1}$ keV, perfectly consistent with the RGS model. The relative emission measure ratio of the hotter to the cooler component dropping from 6:1 at angular distances R = 30–60 arcsec to 1.3:1 inside 15 arcsec. There is little evidence for cool, $kT < 3$ keV, gas outside 90 arcsec in the EPIC spectra. In these two component fits there is no change in the temperature of the cooler component with radius. Fitting a cooling flow model (model *mkcflow* in XSPEC) to the same regions, we find that the minimum temperature in the cooling flow is $kT \sim 1.6$ keV, as is often found in fits of cooling flow models to *XMM-Newton* and *Chandra* data.

5. Discussion

We have found evidence that the low temperature X-ray emission lines of O VIII, Si XIV and Fe XXIII from Abell 2597 have a different redshift to the high temperature lines of Fe XXIV. In this section we exclude the possibility of systematic bias to the redshift measurements, compare our results to data at other wavelengths, and discuss these findings in the context of cooling flows, group mergers and the influence of a central, active nucleus.

5.1. Pointing uncertainties

In this section we briefly discuss whether the measured RGS velocities can be affected by telescope pointing bias. There is a small discrepancy between the location of the cD galaxy in the Digitized Sky Survey (spatially consistent with the brightest knot in the high resolution *Chandra* ACIS image; Fabian et al. 2001) and the position of the source in the OM images. This is most likely a symptom of the telescope pointing accuracy, which is limited to ~ 5 arcsec. With a position angle of 247 degrees, the disparity is ~ 0.4 arcsec in the dispersion direction of the RGS detector. To determine what effect an off-axis pointing on these scales will have on the point-source wavelength scale, we consider the derivative of the dispersion equation:

$$\Delta\lambda = d \sin\alpha_0 \Delta\alpha \quad (1)$$

using a nominal incidence angle of $\alpha_0 = 1.5762$ degrees and a grating groove density of $d^{-1} = 645.6$ lines mm^{-1} (den Herder 2001). After correction for optical geometry, the angular discrepancy is $\Delta\alpha = 0.45$ arcsec. This yields a drift in the wavelength scale at OVIII Lyα of $\Delta\lambda = 1$ mÅ. The redshift difference of our two model components at the wavelength of the OVIII line corresponds to $\Delta\lambda \simeq 0.1$Å. For pointing inaccuracies to contribute significantly to our measurements, we require a pointing offset of order 48 arcsec. Therefore the effect of pointing uncertainties are negligible.

5.2. Cluster velocity distribution

It is constructive to compare the two measured RGS velocities above with the redshift distribution of Abell 2597 cluster members. The often cited redshift of the cluster, $z = 0.0852$, is taken from the catalogue of Struble and Rood (1999) and it originates from the optical radial velocities of only three cluster members, corrected to the Local Group standard of rest (Kowalski, Ulmer and Cruddace 1983). None of these sources are the cD galaxy. To similarly correct our own results to the Local Group, we must add 140 km s^{-1} (Courteau and van den Bergh 1999). This removes just 10 percent of the discrepancy between the cool X-ray lines and the Struble & Rood (1999) redshift. The standard deviation between the three galactic velocities, $z = 2\times10^{-3}$, is of the same order as the difference between our two RGS velocities, but also of the same order as the systematic uncertainty introduced by using different cross-correlation templates in the optical redshift measurements.

The recent availability of the the 2dF galaxy survey data has allowed a drastic improvement in the measurement of the redshift and distribution of galaxy velocities (De Propris et al. 2002). Using the latest 2dF data release, we find 44 galaxies within 30 arcmin of the center of Abell 2597 and their redshift distribution is shown in Fig. 5. It is immediately clear that there are 2 redshift peaks which correspond to the velocities seen in the RGS

TABLE 1

BEST FIT PARAMETERS FOR THE INNER, POINT-LIKE COMPONENT OF THE TWO-ZONE EMISSION MODEL FOR ABELL 2597. OUTER ZONE PARAMETERS HAVE BEEN FIXED USING EPIC MEASUREMENTS AND THE REDSHIFT OF THE OUTER ZONE COMES FROM STRUBLE AND ROOD (1999).

$kT_{\rm i}$	$1.6^{+0.2}_{-0.1}$ keV
[Fe/H]	$-0.32^{+0.16}_{-0.17}$
[O/H]	$-0.46^{+0.29}_{-0.76}$
[Si/H]	$+0.08^{+0.15}_{-0.23}$
$N_{\rm o}/N_{\rm i}$[a]	$5.6^{+0.8}_{-0.4}$
$z_{\rm i}$	$0.0808^{+0.0007}_{-0.0022}$

[a]ratio of emission measures for the two zones.

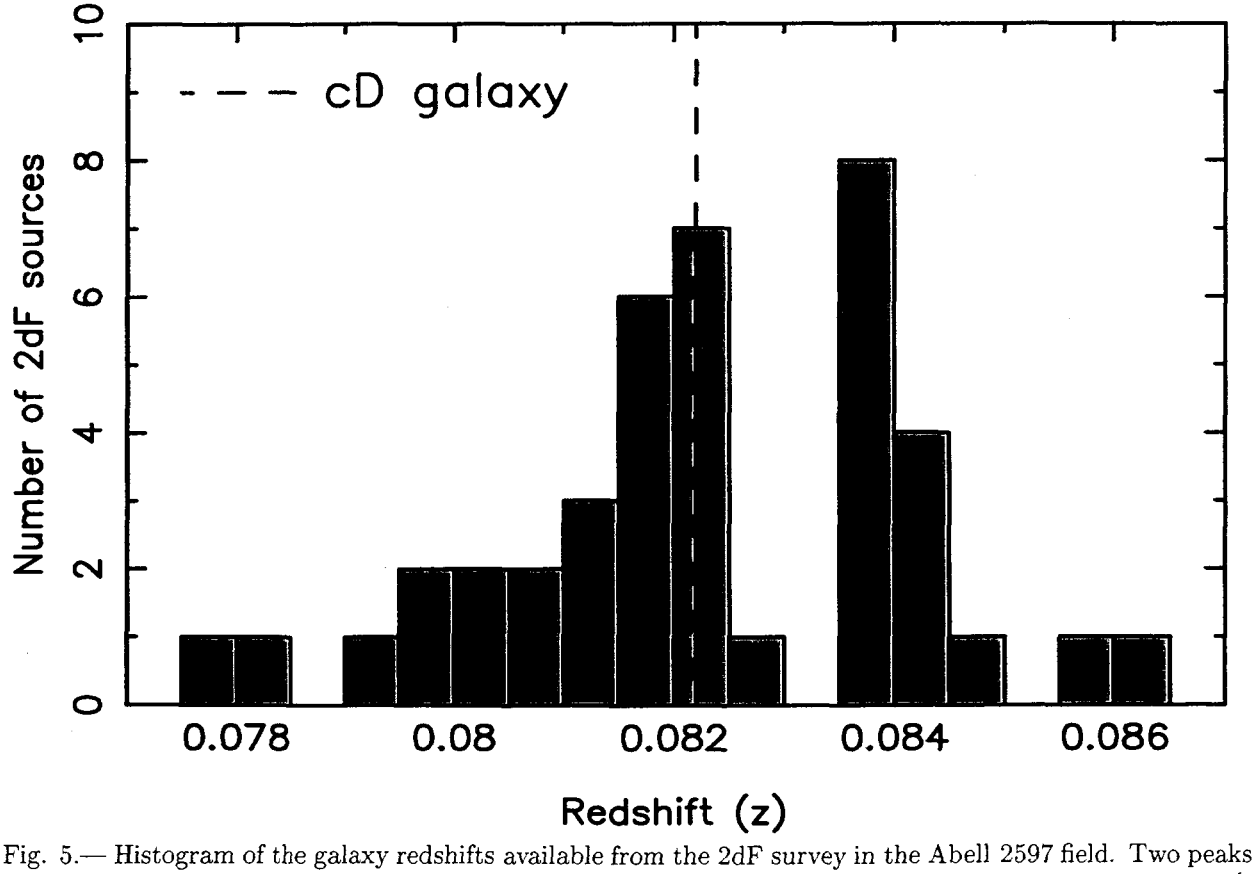

Fig. 5.— Histogram of the galaxy redshifts available from the 2dF survey in the Abell 2597 field. Two peaks in the redshift distribution are found, $z \simeq 0.082$, consistent with the cool component of the RGS model, and $z \simeq 0.084$, consistent with the hot component. The dashed line corresponds to the redshift of the cD galaxy, $z = 0.0822$ (Owen, Ledlow and Keel 1995).

data. The lower redshift peak is the one published by De Propris et al. (2002) and the higher peak is the one cataloged by Struble and Rood (1999). The lower redshift system is also consistent with the velocity of OVI (Oegerle et al. 2001), the radial velocity of the cD galaxy itself of $z = 0.0822$ (Owen, Ledlow and Keel 1995), the velocity of HI seen in absorption against the radio source (O'Dea, Baum and Gallimore 1994), and the velocity of Lyα seen in the archival STIS data. We make a cut in the galaxy redshift distribution at $z = 0.083$ and throw away sources with $z < 0.06$ or $z > 0.1$. Plotting the positions on the sky of the two velocity groups in Fig. 6, we find no segregation in right ascension or declination. This indicates that the velocity structure is approximately orthogonal to the plane of the sky.

5.3. Interpretation

We report, for the first time, significant velocity differences between ion species in the hot X-ray emitting gas in a cluster. The velocity differences between the lines produced in gas with $kT < 2$ keV and the Fe XXIV lines produced at higher effective temperatures is $\Delta z = (4.4^{+2.2}_{-0.7}) \times 10^{-3}$ or $1\,320^{+660}_{-210}$ km s^{-1}, and is significant at > 99 percent confidence. This velocity separation is completely consistent with the observed bi-modal galaxy velocity distribution (Fig. 5), and the lower-velocity, cooler gas lies at the redshift of the cD galaxy. This range in gas velocity is slightly supersonic since the sound speed is $\sim$ 950 km s^{-1}for the $kT = 3.5$ keV gas which constitutes the bulk of the cluster emission.

At shorter wavelengths, the HI absorption spectrum towards Abell 2597 shows complex velocity structure over the central 3 arcsecs (O'Dea, Baum and Gallimore 1994), similar to that detected in the Perseus cluster. Projected across the nucleus is a clump, infalling by ~ 300 km s^{-1} (as opposed to our outflow of 1 320 km s^{-1}) and a broad HI absorption ($\sim$ 400 km s^{-1}) relative to the systemic velocity of the cD galaxy at $z = 0.082$. The Hα emission (Heckman et al. 1989) has a velocity width of ~ 600 km s^{-1}, but is also at the systemic velocity. Thus while there is strong evidence of velocity turbulence and shear in Abell 2597 from radio and optical data, neither reveal evidence for redshifted gas. There is also no evidence in the OVI or Lyman alpha emission for the higher redshift component. We thus associate the lower redshift gas with the velocity of the cD and its associated galaxies.

5.3.1. Cluster merger

The cool gas velocity relative to the hot gas is quite consistent with with the observed galaxy distribution and projected velocities predicted in many numerical simulations. As first reported in Roettiger, Burns and Loken (1996), the gas in the lower temperature merging groups remains bound to the group for a considerable length of time. Thus it is possible that a "cool" core is, in reality, a projection of a merging group as it falls into a rich cluster. If this is so, this gas would be expected to retain the velocity of its infall for a considerable period of time. This scenario is discussed in detail by Motl et al. (2004), who predict that many of the "cooling flows" observed are in reality projections of infalling groups. To first order in this model, one predicts velocity shear across the center of the cluster due to projection effects, where the observed cool core is due to emission of an infalling group, projected against the cluster center. This idea is also consistent with the relative lack of cooling gas seen in the *XMM-Newton* RGS spectra of many clusters (Peterson et al. 2003). However, as stressed by Motl et al. , while the predicted velocity structure is quite complex, material is always streaming through the cluster core. Thus the Motl et al. results are not well described by our simple model of two components to the velocity structure. However it is clear that the merging model for cooling flows naturally predicts the velocity structure seen in our analysis and allows a natural interpretation of the data.

There are reasons to doubt this interpretation. The X-ray image and temperature map (Fig. 1) show little structure with the X-ray isophotes being slightly elongated in the NW–SE direction, consistent with the galaxy distribution direction. We have quantified this statement by extracting spectra from regions of the X-ray color image that deviate by more than 1σ from the mean color and with more than 2000 counts in the PN spectrum. We find no evidence for temperature structure beyond that given by statistical error, with each region having internal errors of approximately ± 0.5 keV. Both the *XMM-Newton* and *Chandra* (Fabian et al. 2001) azimuthally av-

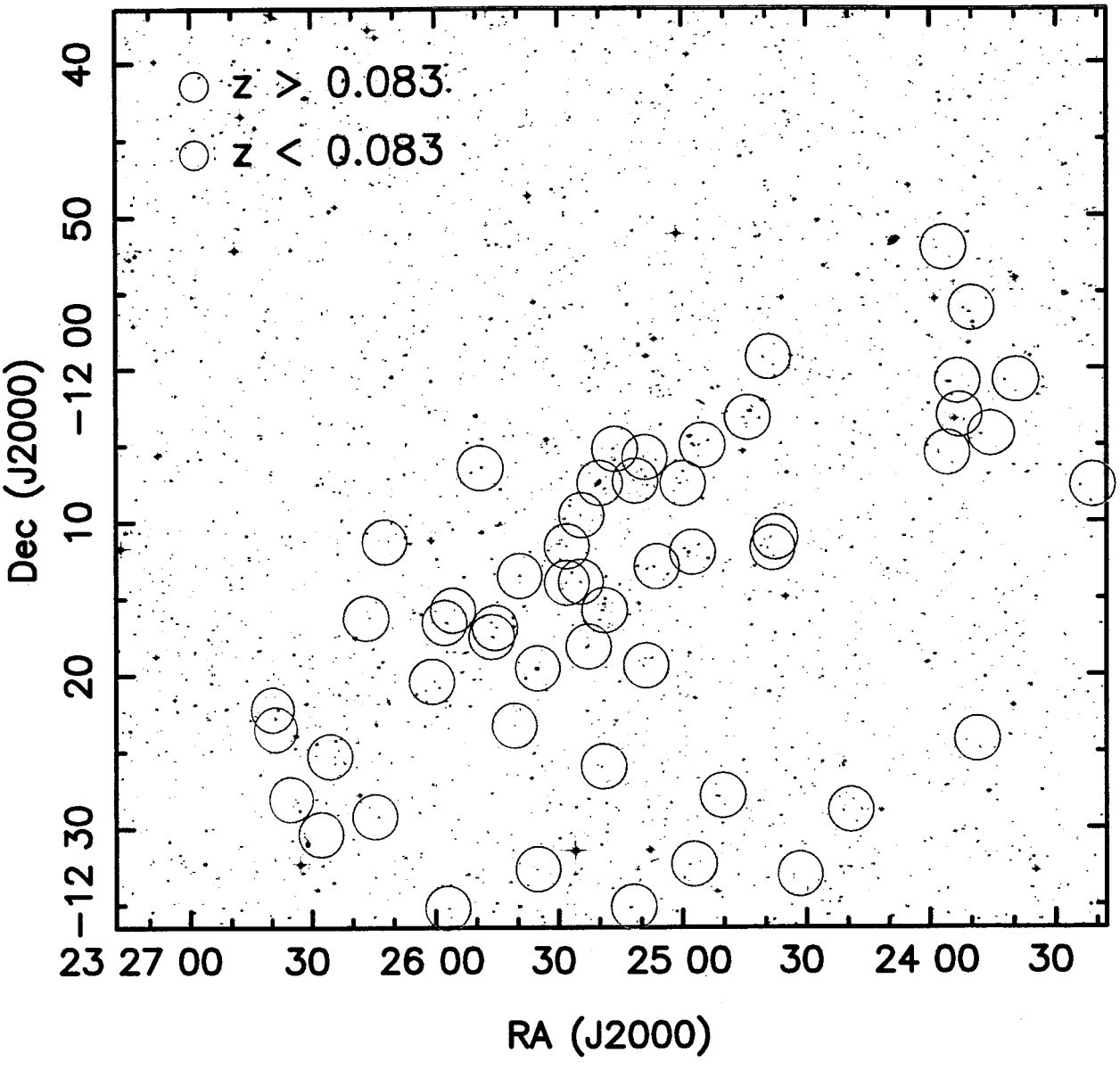

Fig. 6.— Positions of sources within the 2dF survey have been plotted over a digitized plate from the Palomar sky survey. Source with $z < 0.06$ or $z > 0.1$ have been omitted. Remaining galaxies have been segregated into two redshift bins, where the division is made at $z = 0.083$. The two populations do not have different distributions on the sky. The cD galaxy is listed in the 2dF survey and is centered in the image.

eraged temperature profiles show that there is a significant reduction in cluster temperature only in the central 1 arcmin. Thus if there is an infalling group it has to be rather small, < 1 arcmin in projected size (~ 100 kpc), and well centered on the overall X-ray surface brightness isophotes. While this seems rather unlikely, the probability of detecting a purely radial inflow of a group along a filament is not well known. Norman and Bryan (1999) estimate using the Lacey et al. (1993) merger tree that an appropriate minor merger occurs every 0.4 Gyr, and that the velocities decay on a similar time scale. Since cool cores in clusters are very common, this seems quite reasonable, but the relative solid angle of inflows along filaments has not been well determined.

The observed galaxy distribution within Abell 2597 (Trevese et al. 1992) is highly elongated in the plane of the sky (Fig 7), consistent with seeing a filament at a large inclination angle. We thus speculate that the combination of the X-ray velocity structure, galaxy velocity distribution, lack of X-ray temperature structure and galaxy distribution can be explained by a fortunate set of circumstances in which we are observing a merger of two objects at a very oblique angle to the plane of the sky, and in which there are no strong shocks in the merger. However a large compilation of simulated clusters (http://sca.ncsa.uiuc.edu) shows that such occurrences may be rare.

5.3.2. Central engine

Alternatively the velocity of the cool central region could be due to the effects of an active galaxy. In most of the Chandra spectral images of X-ray emission influenced by the central radio source (e.g. Belsole et al. 2001; Fabian et al. 2002; Blanton, Sarazin and McNamara 2003), the region around the radio emitting plasma is cooler than the surrounding gas. The central galaxy of Abell 2597 (Sarazin et al. 1995) is a luminous radio source and there are indeed "cavities" in the X-ray emission similar to those seen in Perseus and Abell 2052 (McNamara et al. 2001). However, analysis of the Chandra hardness ratios shows that the emission immediately adjacent to each cavity is generally no harder or softer than its surroundings (McNamara et al. 2001) . In addition, in neither the Chandra nor *XMM-Newton* images is there evidence for a central point source indicating that the present day luminosity of a central AGN is rather low. As noted in McNamara et al. , if the X-ray cavities are due to buoyant bubbles, they must rise in the central regions on timescale of $10^{7.7} - 10^{8}$ yrs, and thus have a velocity of 300–500 $\mathrm{km\,s^{-1}}$. This is somewhat slower than our observed velocity. However, since we see the bubbles projected in the plane of the sky, the true velocity may be larger.

In the numerical simulations of Reynolds et al. (2002) and Bruggen (2003) one clearly sees velocity structure still present long after the radio source has turned off. In the Omma et al. (2003) simulations, velocities of up to 4 000 $\mathrm{km\,s^{-1}}$ are obtained by X-ray emitting gas along the axes of jets, even at distances of ~ 50 kpc from the center. It is not clear in this scenario what the origin of the single velocity shift we observe is, since one expects more velocity broadening than velocity shifts. However as these authors point out, about 17 Myr after the jet turns off, the vortex fills and overtakes the cavity, which is thus replaced by a region of outward-moving, cool, overdense gas, which may produce our observed outgoing velocity structure.

An alternative source of high velocity gas is the copious star formation occurring in the central regions of Abell 2597 (Koekemoer et al. 2002), in which case we may be observing the equivalent of a "blowout" in a starburst galaxy. However, since the gas is expanding into a hot dense environment in this case, the boundary conditions are rather different and it is not clear what the velocity field should be.

It is tempting to speculate, based on the Chandra and *XMM-Newton* results for the Perseus cluster (e.g. Fabian et al. 2003, Churazov et al. 2004; Gastaldello and Molendi 2004), and the Chandra images of Abell 2597 (McNamara et al. 2000), that our observed velocity structure is due to turbulence in the inter-galactic medium, related to the presence of the radio structure. However this would then not explain the coincidence with the velocity structure seen in the galaxies.

5.4. Effects on cooling flow models

The effect of velocity structure on models of cooling flows is severe. Abell 2597 had an inferred cooling rate of ~ 300–400 $\mathrm{M_\odot}$ per year (Crawford

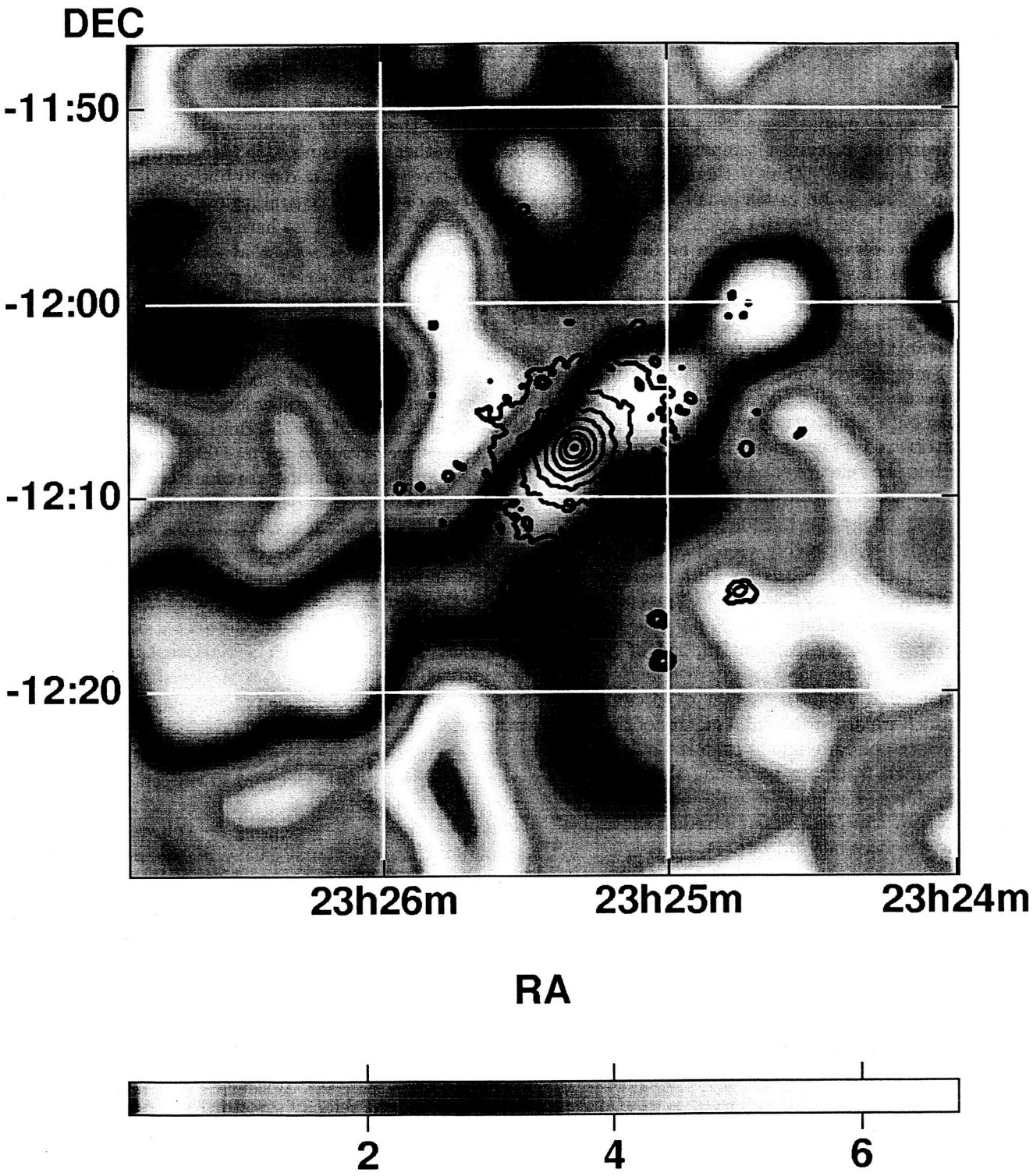

Fig. 7.— A contour map of the *XMM-Newton* EPIC MOS1 image overlayed on a density map of galaxies. Sources were identified from the Palomar survey by Trevese et al. (1992). We smoothed the galaxy map by a Gaussian function of FWHM 9.1 arcmin.

et al. 1989) inside a cooling radius of $\sim$ 1–2 arcsec (Sarazin and McNamara 1997). Spectral analysis of both the EPIC and RGS data show the, by now common, absence of gas cooler than $\sim 1/3$ of the asymptotic cluster temperature of 3.5 keV. However we now know that most of the cool gas has a different redshift compared to the gas hotter than 2 keV. Thus for the $kT \sim 3.5$ keV gas to "cool" and become the $kT < 2$ keV gas, it must also change its redshift, which seems rather unlikely. Thus, in this cluster, we can reject the idea of cooling from our dynamical data. This decomposition of the cluster emission argues that most of the mass in Abell 2597 resides in the higher redshift, hot component because we see little emissivity from the cool compact component, in the RGS data. However, a large fraction of all the galaxy redshifts are consistent with the lower velocity cool component. It thus seems rather likely that Abell 2597 has not reached equilibrium between the distribution of galaxies and gas. While it is, at present, unknown how often "cool cores" have a different velocity from the surrounding hot gas, the effect we see in our data is rather subtle and may have been missed in previous analyses of the RGS cluster data (e.g. Peterson et al 2003).

6. Conclusion

We detect for the first time significant velocity differences between different X-ray emitting ions in the core of a rich cluster. The lower temperature gas is moving at $\sim -1\,320$ km s^{-1} with respect to the hotter component. The cool components redshift is consistent with the optical and radio emitting gas near the central cD and one of the two galaxy velocity clumps. The hot components velocity is consistent with the higher redshift clump of galaxies. This agreement between the X-ray and optical velocities argues that Abell 2597 is a merger more or less into the plane of the sky. The relative emission measures of the cool and hot components shows that the bulk of the X-ray emissivity is associated with the higher velocity component. The different velocities between the cool and hot components argues that this object is not a cooling flow (in the sense that cooling of the hot gas produces the cool gas) and that a more likely origin of the cool gas is a merging group. It seems less likely, at least in this cluster, that the velocity shear is due to the effects of an active galaxy.

Further analysis of more *XMM-Newton* RGS data and the higher signal to noise and resolution data from Astro-E2 will show whether Abell 2597 is unique.

Based on observations obtained with *XMM-Newton*, an ESA science mission with instruments and contributions directly funded by ESA Member States and the USA (NASA). The Digitized Sky Survey was produced at the Space Telescope Science Institute under U.S. Government grant NAG W-2166. The images of these surveys are based on photographic data obtained using the Oschin Schmidt Telescope on Palomar Mountain and the UK Schmidt Telescope. The plates were processed into the present compressed digital form with the permission of these institutions. The *rgsxsrc* model was authored by A. Rasmussen. We thank J. Peterson for the use of his Monte Carlo fitting code.

REFERENCES

Arnaud M., Rothenflug R., 1985, A&AS, 60, 425

Balucinska-Church M., McCammon D., 1992, ApJ, 400, 699

Belsole E. et al., 2001, A&A, 365, L188

Blanton E.L., Sarazin C.L., McNamara B.R., 2003, ApJ, 585, 227

Brickhouse N.S., Dupree A.K., Edgar R.J., Liedahl D.A., Drake S.A., White N.E., Singh K.P., 2000, ApJ, 530, 387

Brown G.V., Beiersdorfer P., Liedahl D.A., Widmann K., Kahn S.M., Clothiaux E.J., 2002, ApJS, 140, 589

Bruggen M., 2003, ApJ, 592, 839

Burns J.O. et al., 2002, NewAR, 46, 135

Churazov E., Forman W., Jones C., Böhringer H., 2000, A&A, 356, 788

Churazov E., Forman W., Jones C., Sunyaev R., Böhringer H., 2004, MNRAS, in press

Courteau S., van den Bergh S., 1999, AJ, 118, 337

Crawford C.S., Fabian A.C., Johnstone R.M., Arnaud K.A., 1989, MNRAS, 236, 277

De Propris R. et al., 2002, MNRAS, 329, 87

Dickey J.M., Lockman F.J., 1990, ARAA. 28, 215

den Herder J.W. et al., 2001, A&A, 365, L7

Fabian A.C. et al., 2003, MNRAS, 344, L43

Fabian A.C., Celotti A., Blundell K.M., Kassim N.E., Perley R.A., 2002, MNRAS, 331, 369

Fabian A.C. et al., 2001, MNRAS, 321, L33

Gastaldello F., Molendi S., 2004, ApJ, in press

Heckman T.M., Baum S.A., van Breugel W.J.M., McCarthy P., 1989, ApJ, 338, 48

Jansen F. et al., 2001, A&A, 365, L1

Johnson W.R., Soff G., 1985, Atom. Data Nucl. Data Tables, 33, 405

Koekemoer A.M. et al., 2002, NewAR, 46, 149

Kowalski M.P., Ulmer M.P., Cruddace R.G., 1983, ApJ, 268, 540

Lacey C., Guiderdoni B., Rocca-Volmerange B., Silk J., 1993, ApJ, 402, 15

Mason K.O. et al., 2001, A&A, 365, L36

McNamara B.R. et al., 2001, ApJ, 562, L149

Motl P.M., Burns J.O., Loken C., Norman M.L., Bryan G., 2004, ApJ, in press

Mushotzky R.F. et al., 2004, in prep.

Nagai D., Kravtsov A.V., 2003 ApJ, 587, 514

Norman M.L., Bryan G.L., 1999, p. 106 in Röser H.-J., Meisenheimer K., eds., The radio galaxy Messier 87, Berlin:Springer

O'Dea C.P., Baum S.A. Gallimore J.F., 1994, ApJ, 436, 669

Oegerle W.R. et al., 2001, ApJ, 560, 187

Omma H., Binney J., Bryan G., Slyz A., 2004, MNRAS, in press

Onuora L.I., Kay S.T., Thomas P.A., 2003, MNRAS, 341, 1246

Owen F.N., Ledlow M.J., Keel W.C., 1995, AJ, 109, 14

Peterson J.R. et al., 2001, A&A, 365, L104

Peterson J.R. et al., 2003, ApJ, 590, 207

Reynolds C.S., Heinz S., Begelman M.C., 2002, MNRAS, 332, 271

Roettiger K, Burns J.O., Loken C., 1996, ApJ, 473, 651

Roettiger K., Stone J.M., Mushotzky R., 1998, ApJ, 493, 62

Sarazin C.L., Burns J.O., Roettiger K., McNamara B.R., 1995, ApJ, 447, 559

Sarazin C.L., McNamara B.R., 1997, ApJ, 480, 203

Stoughton C. et al., 2002, AJ, 123, 485

Struble M.F., Rood H.J., 1999, ApJS, 125, 35

Strüder L. et al., 2001, A&A, 365, L18

Trevese D., Flin P., Migliori L., Hickson P., Pittella G., 1992, A&AS, 94, 327

Turner M.J.L. et al., 2001, A&A, 365, L27

Xu H. et al., 2002, ApJ, 579, 600

This 2-column preprint was prepared with the AAS LaTeX macros v5.0.